Article

Cell Reports

Vaccination with Necroptotic Cancer Cells Induces Efficient Anti-tumor Immunity

Graphical Abstract

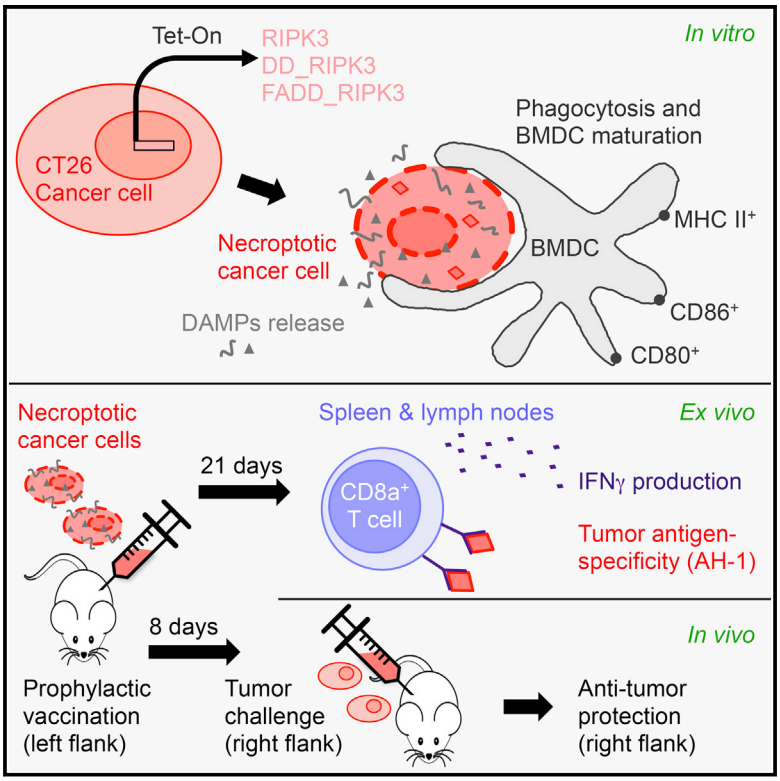

Highlights

- Necroptotic cancer cells release DAMPs and induce dendritic cell maturation in vitro
- Cross-priming of T cells was induced by necroptotic cancer cells in vivo
- Necroptotic cancer cells promote the tumor antigen-specific production of IFN-γ ex vivo
- Prophylactic injection of necroptotic cancer cells leads to an anti-tumor vaccination

Authors

Tania Løve Aaes, Agnieszka Kaczmarek, Tinneke Delvaeye, ..., Wim Declercq, Peter Vandenabeele, Dmitri V. Krysko

Correspondence

peter.vandenabeele@irc.vib-ugent.be

In Brief

Løve Aaes et al. show that necroptotic cancer cells induce the maturation of dendritic cells, the cross-priming of cytotoxic T cells, and the production of IFN-γ in response to tumor antigen stimulation. Using RIPK3 induction systems, the authors further demonstrate efficient prophylactic vaccination with immunogenic necroptotic cells.

Aaes et al., 2016, Cell Reports *15*, 1–14
April 12, 2016
http://dx.doi.org/10.1016/j.celrep.2016.03.037

CellPress

Please cite this article in press as: Aaes et al., Vaccination with Necroptotic Cancer Cells Induces Efficient Anti-tumor Immunity, Cell Reports (2016), http://dx.doi.org/10.1016/j.celrep.2016.03.037

Cell Reports
Article

Vaccination with Necroptotic Cancer Cells Induces Efficient Anti-tumor Immunity

Tania Løve Aaes,[1,2] Agnieszka Kaczmarek,[1,2] Tinneke Delvaeye,[1,2,3] Bram De Craene,[2,4] Stefaan De Koker,[2,5] Liesbeth Heyndrickx,[1,2] Iris Delrue,[1,2] Joachim Taminau,[2,4] Bartosz Wiernicki,[1,2] Philippe De Groote,[1,2] Abhishek D. Garg,[6] Luc Leybaert,[3] Johan Grooten,[2,5] Mathieu J.M. Bertrand,[1,2] Patrizia Agostinis,[6] Geert Berx,[2,4] Wim Declercq,[1,2] Peter Vandenabeele,[1,2,7,8,*] and Dmitri V. Krysko[1,2,8]

[1]Molecular Signaling and Cell Death Unit, Inflammation Research Center, VIB, 9052 Ghent, Belgium
[2]Department of Biomedical Molecular Biology, Cancer Research Institute Ghent (CRIG), Ghent University, 9052 Ghent, Belgium
[3]Physiology Group, Department of Basic Medical Sciences, Ghent University, 9000 Ghent, Belgium
[4]Molecular and Cellular Oncology Unit, Inflammation Research Center, VIB, 9052 Ghent, Belgium
[5]Department of Pharmaceutics, Ghent University, 9000 Ghent, Belgium
[6]Cell Death Research and Therapy Lab, Department of Cellular and Molecular Medicine, KU Leuven - University of Leuven, 3000 Leuven, Belgium
[7]Methusalem Program, Ghent University, 9000 Ghent, Belgium
[8]Co-senior author
*Correspondence: peter.vandenabeele@irc.vib-ugent.be
http://dx.doi.org/10.1016/j.celrep.2016.03.037

SUMMARY

Successful immunogenic apoptosis in experimental cancer therapy depends on the induction of strong host anti-tumor responses. Given that tumors are often resistant to apoptosis, it is important to identify alternative molecular mechanisms that elicit immunogenic cell death. We have developed a genetic model in which direct dimerization of FADD combined with inducible expression of RIPK3 promotes necroptosis. We report that necroptotic cancer cells release damage-associated molecular patterns and promote maturation of dendritic cells, the cross-priming of cytotoxic T cells, and the production of IFN-γ in response to tumor antigen stimulation. Using both FADD-dependent and FADD-independent RIPK3 induction systems, we demonstrate the efficient vaccination potential of immunogenic necroptotic cells. Our study broadens the current concept of immunogenic cell death and opens doors for the development of new strategies in cancer therapy.

INTRODUCTION

The discovery of immunogenic apoptosis (IA) underlines the importance of tumor-host interaction, in which the activation of an immune response, specifically toward malignant cancer cells, results in a potent and long-lasting anti-cancer immunity (Casares et al., 2005). IA is characterized by the release of damage-associated molecular patterns (DAMPs), such as cell-surface exposure of calreticulin (Garg et al., 2012a; Obeid et al., 2007a), secretion of ATP (Garg et al., 2012b; Ghiringhelli et al., 2009; Michaud et al., 2011), and release of the chromatin-binding protein high-mobility group B1 (HMGB1) (Apetoh et al., 2007; Yamazaki et al., 2014), each of which interact with the phagocytic or scavenger receptors, e.g., LRP1 (calreticulin), purinergic receptors (ATP), and pattern-recognition receptors, such as TLR4 (HMGB1), respectively. Thus, inducing IA in cancerous cells can be very beneficial in a therapeutic setting because DAMPs induce a host anti-tumor immune response. However, in order to overcome apoptosis resistance, which is often observed in tumors (Hanahan and Weinberg, 2011), it is of great importance to find other ways to kill tumor cells by triggering cell death modalities different from apoptosis.

Necrosis has long been described as a consequence of extreme physiochemical stress, such as osmotic shock and freezing-thawing (referred to throughout the text as "F/T"), and was therefore classified as uncontrolled or accidental cell death (Kaczmarek et al., 2013). However, more recent findings have demonstrated many different cellular stimuli that induce regulated forms of necrosis, which follow defined steps and signaling events reminiscent of a true cell death program. Necroptosis is one form of regulated necrosis and is mediated by receptor-interacting protein kinase-1 (RIPK1), RIPK3, and its substrate mixed lineage kinase domain-like (MLKL) and has been reported to contribute to inflammation under pathological conditions (Degterev et al., 2005; He et al., 2013; Holler et al., 2000; Pasparakis and Vandenabeele, 2015; Pierdomenico et al., 2014).

In this study, we evaluated the immunogenicity of necroptosis and tested its potential as an alternative approach in cancer therapy. We observed that cancerous CT26 cells undergoing necroptosis can be immunogenic in vitro and in vivo, where the necroptotic cells served as potent immunizers in a prophylactic tumor vaccination model. Vaccination with necroptotic cancer cells effectively cross-primed cytotoxic $CD8a^+$ T cells in vivo and elicited the strong CT26 tumor antigen-specific production of IFN-γ ex vivo. The immunogenicity of necroptotic cells did not correlate with the extent of NF-κB activation. These findings identify necroptotic cancer cells as efficient inducers of an adaptive immune response and show that necroptosis can be

Please cite this article in press as: Aaes et al., Vaccination with Necroptotic Cancer Cells Induces Efficient Anti-tumor Immunity, Cell Reports (2016), http://dx.doi.org/10.1016/j.celrep.2016.03.037

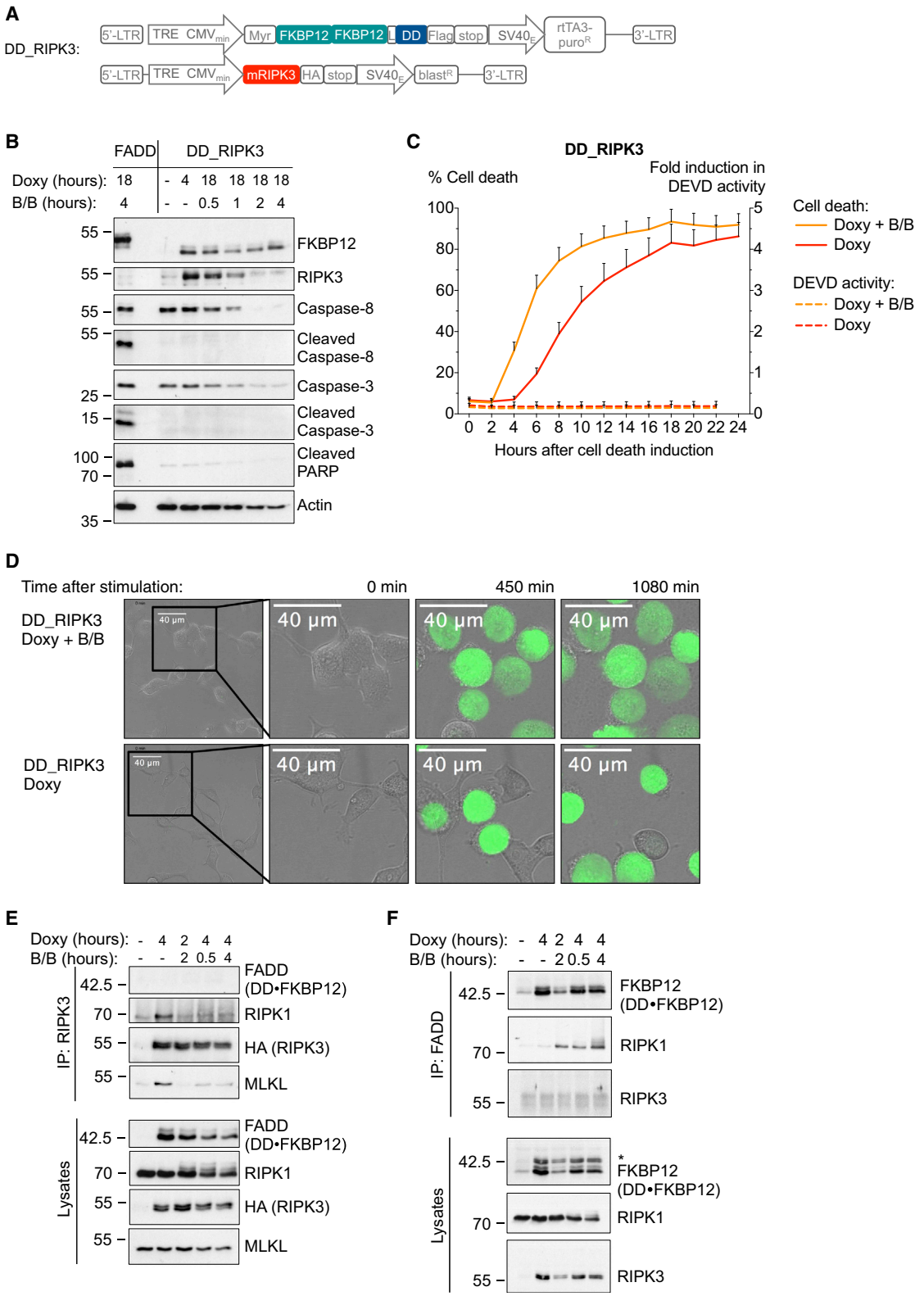

Figure 1. Generation of a Tet-On-Inducible Ligand-free Model of Necroptosis in Murine Tumor Cells

(A) Schematic presentation of the Tet-On-inducible constructs introduced into the CT26 cells (DD_RIPK3). A myristoylation signal (Myr), two copies of FKBP12, a linker (L) to allow flexible dimerization, and the death domain (DD) of FADD. In a separate vector: full-length murine RIPK3, followed by an HA tag.

(legend continued on next page)

Table 1. An Overview of the Inducible CT26 Cell Lines Made for This Study, and Their Mode of Action on Stimulation with B/B Homodimerizer and/or Doxycycline

CT26 Clone Name	Treatment to Induce Cell Death	Dimerization upon Addition of B/B	Cell Death Mode
FADD_RIPK3	doxycycline + B/B dimerizer	FADD	necroptosis
DD_RIPK3	doxycycline + B/B dimerizer	DD	necroptosis
DD_RIPK3	doxycycline	DD	necroptosis
RIPK3	doxycycline	–	necroptosis

as immunogenic as known immunogenic apoptosis inducers, such as mitoxantrone.

RESULTS

Generation of a Tet-On-Inducible Ligand-free Model of Necroptosis in Murine Tumor Cells

Necroptosis is commonly induced by ligand-dependent activation of certain members of the TNFR and TLR families (Vanlangenakker et al., 2011). To circumvent the use of cell death-inducing ligands or other immune active molecules that would not allow us to evaluate the immune response resulting uniquely from necroptosis induction, we opted for the use of inducible Tet-On systems for the expression of the downstream necroptotic effector proteins, allowing us to induce necroptosis independently of any receptor activation. We, and others, previously reported that induced expression and dimerization of the death domain (DD) of FADD is sufficient to induce RIPK1-dependent necroptosis in certain cells (Lohmann et al., 2009; Vanden Berghe et al., 2004). Therefore, we initially tested this strategy in the BALB/c mouse-derived CT26 cells, a colon carcinoma cell line, which is commonly used to analyze the immunogenicity of apoptosis-inducing drugs or cellular stress-inducing conditions (Apetoh et al., 2007; Casares et al., 2005; Garg et al., 2012b; Ghiringhelli et al., 2009; Michaud et al., 2011). For this purpose, a doxycycline (doxy)-inducible vector containing the DD of FADD, coupled to two FKBP12 domains (which allows DD multimerization on addition of a homodimerizer referred to as B/B), was introduced into the murine CT26 cells. However, we found that, in contrast to other cell lines, the mere expression and dimerization of DD in CT26 cells did not induce cell death (data not shown). We found out that this difference originates from the fact that RIPK3 is not expressed in the CT26 cells. In order to circumvent this deficiency, we introduced a doxy-inducible vector containing RIPK3 in addition to the DD-containing construct (Figure 1A; Table 1). Stimulation of these cells (referred to as DD_RIPK3) with doxy triggered caspase-independent cell death (Figures 1B and 1C), which is accelerated in the presence of B/B (Figure 1C). Phase-contrast and time-lapse microscopy (Figure 1D; Movies S1 and S2) further revealed rounding up and swelling of cells (oncosis) and plasma membrane permeabilization, two hallmarks of necrotic cell death (Majno and Joris, 1995). Immunoprecipitation of RIPK3 shows that necroptosis induction is associated with the formation of a complex consisting of RIPK1, RIPK3, and MLKL (Figure 1E) (Cho et al., 2009; He et al., 2009; Li et al., 2012; Pasparakis and Vandenabeele, 2015; Sun et al., 2012). Surprisingly, the additional multimerization of the DD domains of FADD, which results in accelerated necroptosis (Figure 1C), did not increase but instead decreased the interaction of RIPK3 with RIPK1 and MLKL (Figure 1E). In contrast, DD multimerization greatly enhanced recruitment of RIPK1 to FADD (Figure 1F) and seems to be associated with RIPK1 modifications, which have previously been reported to correlate with RIPK1-induced death (Dondelinger et al., 2013; Dynek et al., 2010). Importantly, we found that RIPK1 was required for cell death induction in the absence of forced DD multimerization (Figures S1A and S1E). Repression of MLKL (Figure S1E) did not block cell death progression (Figures S1A and S1C), but rather induced a switch to apoptosis, both in the presence and in the absence of forced DD multimerization (Figures S1B and S1D), as previously described for TNF-induced necroptosis (Remijsen et al., 2014). Additionally, we detect phosphorylation of MLKL on Ser345 (Murphy et al., 2013; Wang et al., 2014) upon stimulation with doxy, as well as with doxy + B/B (Figure S1F). All these data suggest the induction of necroptosis in DD_RIPK3 cells in both inducible conditions.

(B) Cells were stimulated with doxycycline for 4 or 18 hr and co-stimulated with B/B, where indicated during the last 0.5–4 hr. Western blot shows no apoptotic features (cleaved Caspase-8, cleaved Caspase-3, or cleaved PARP) during necroptosis induction in the DD_RIPK3 cells. FADD-overexpressing CT26 cells serve as a positive control. In the condition of stimulation with doxy + B/B, pro-caspase-3 and pro-caspase-8 start to disappear upon cell death induction at 1 hr after B/B addition, because these cells were already pre-treated for 18 hr with doxycycline, which induces massive induction of cell death (up to 80% of Sytox$^+$ cells). At this rather late stage of cell death, one characteristic is the degradation of the proteins and their passive release, which has been previously reported (Denecker et al., 2001). In the condition of stimulation with doxy alone for 4 hr, pro-caspase-3 and pro-caspase-8 were still detected on western blot, because this is still an early stage of cell death. Note that CT26 cells do not express RIPK3 in the non-induced conditions. The faint band observed in the unstimulated DD_RIPK3 cells (lane 3) is due to a slight leakiness of the RIPK3 construct. The western blot shown here is representative for one of three independent experiments.

(C) Cell death progression measured by SYTOX Green fluorescence in the DD_RIPK3 cells upon stimulation with doxy or doxy + B/B. No DEVD activity is detected during the cell death progression. Pool of seven independent experiments.

(D) Time-lapse microscopy reveals the permeabilization, but no blebbing, of the plasma membrane during cell death, measured by SYTOX Green and induced by overexpression and dimerization of DD_RIPK3 (upper) or the mere overexpression of DD_RIPK3 (lower). The images are derived from Movies S1 and S2, respectively.

(E) Immunoprecipitation of RIPK3 shows RIPK1-MLKL-RIPK3 complex formation upon doxy-induced necroptosis; this is abolished upon addition of the B/B homodimerizer. The anti-FADD antibody recognizes endogenous FADD (30 kDa), which in this cell line corresponds to the overexpressed DD-FKBP12 protein (42 kDa).

(F) Immunoprecipitation of FADD reveals a FADD-RIPK1 complex upon overexpression of DD_RIPK3, combined with the dimerization of DD. Under this condition RIPK1 modifications are also seen (note the smear above the RIPK1 band at the 4 hr co-induction with doxy and B/B). Without addition of the B/B dimerizer, there is no complex formation. *The remnant RIPK3 band is still visible from the previous membrane exposure.

See also Figure S1 and Movies S1 and S2.

Please cite this article in press as: Aaes et al., Vaccination with Necroptotic Cancer Cells Induces Efficient Anti-tumor Immunity, Cell Reports (2016), http://dx.doi.org/10.1016/j.celrep.2016.03.037

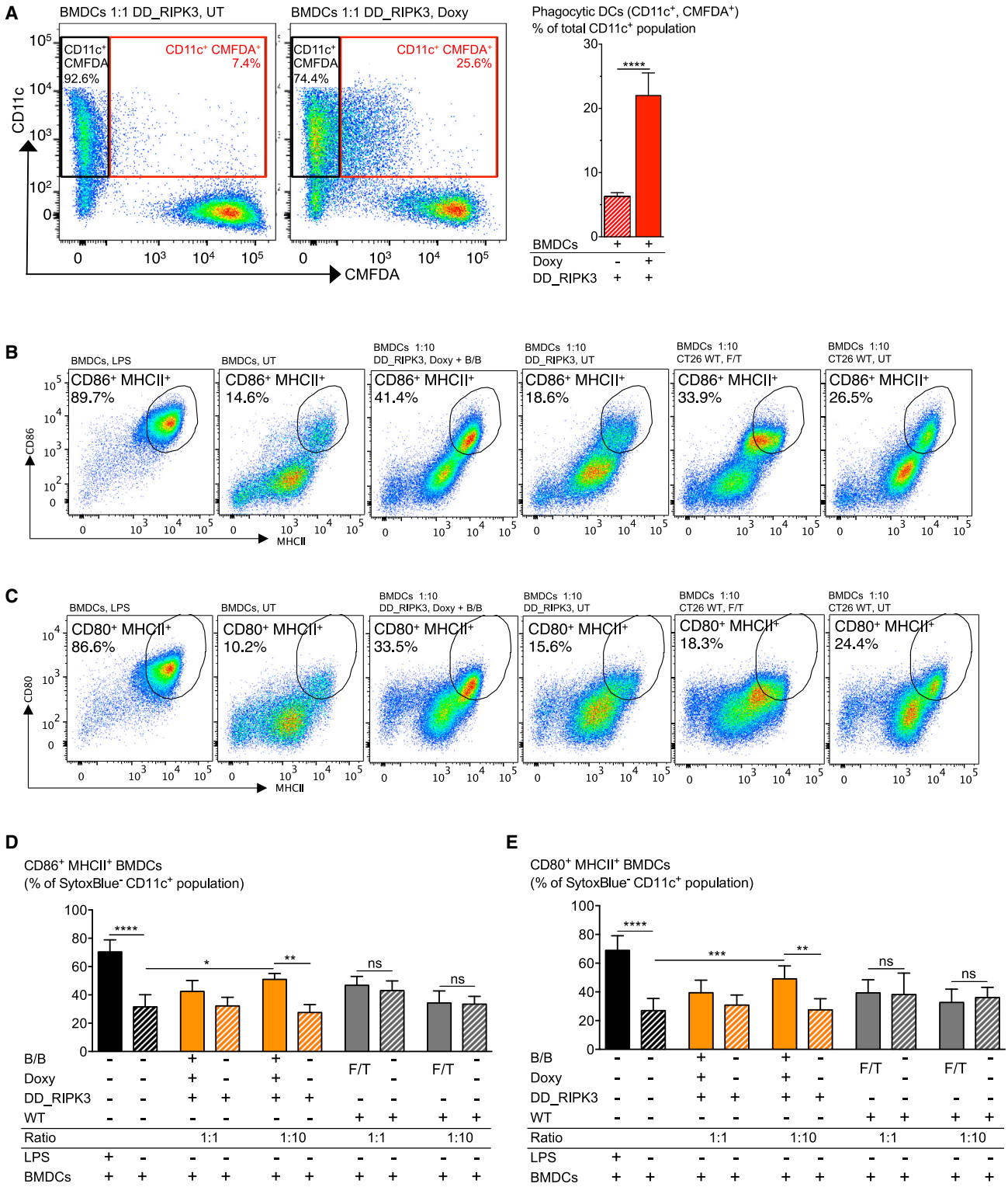

Figure 2. Necroptotic Cancerous Cells Are Phagocytized and Induce BMDC Maturation

(A) Phagocytosis assay shows effective uptake by BMDCs of necroptotic cells killed by doxy. (Left) Representative flow cytometry dot plots show the uptake of CMFDA-labeled dead cell material by BMDCs ($CD11c^+CMFDA^+$ double-positive cells). (Right) The quantification is the pool of triplicates from three independent experiments and represents the mean value + SEM. UT, untreated (live DD_RIPK3) cells.

(legend continued on next page)

Necroptotic Cancerous Cells Are Phagocytized and Induce Bone Marrow-Derived Dendritic Cell Maturation

Next, we tested the immunogenic properties of these necroptotic tumor cells in vitro. By co-culturing untreated DD_RIPK3 cells (live cells) or doxy-treated DD_RIPK3 cells (necroptotic cells) with primary bone marrow-derived dendritic cells (BMDCs), we observed that the necroptotic cells, and not the live cells, were effectively engulfed by BMDCs (Figure 2A). Maturation of DCs is characterized by the upregulation of surface co-stimulatory ligands, of which MHC-II is vital for the priming of naive T cells and for mounting an anti-tumor immune response (Ma et al., 2013). We found that the necroptotic (DD_RIPK3) cells, but not the same amount of live or accidental necrotic (F/T) cells, alter the maturation status of the BMDCs. BMDCs co-cultured with necroptotic cells in a 1:10 ratio showed maturation as indicated by upregulation of the co-stimulatory ligands $MHCII^+CD86^+$ (Figures 2B and 2D) and $MHCII^+CD80^+$ (Figures 2C and 2E) when compared with untreated BMDCs or with BMDCs co-cultured with live DD_RIPK3 cells. Co-culture with the same amount of F/T accidental necrotic cells apparently did not alter the maturation status of BMDCs. Together, these in vitro results indicate that necroptotic DD_RIPK3 cells are potent inducers of BMDC-mediated phagocytic clearance and phenotypic maturation.

Necroptotic Cells Induce Anti-tumor Immunogenicity with the Cross-Priming and Proliferation of $CD8^+$ T Cells

In order to test the ability of necroptotic tumor cells to activate the adaptive immune system, we used a well-established prophylactic tumor vaccination model in immunocompetent BALB/c mice (Figure 3A) (Casares et al., 2005; Garg et al., 2012b; Ghiringhelli et al., 2009; Kepp et al., 2014; Michaud et al., 2011; Obeid et al., 2007a). Immunization of mice with necroptotic DD_RIPK3 cells, induced by doxy and B/B, or by doxy treatment alone, prevented tumor growth at the challenge site (Figures 3B and 3C). Notably, the mice that were vaccinated with the same number of F/T cells remained significantly less tumor-free on the challenge site (Figures 3C and 3D), indicating that accidental necrotic cells apparently are less immunogenic than are necroptotic DD_RIPK3 cells killed by stimulation with doxy. In line with this, the immunogenicity of F/T accidental necrotic tumor cells was completely lost when the mice were immunized with half the amount of cells (Figure 3D), whereas the necroptotic cells remained equally immunogenic, independently of the way necroptosis was elicited, viz. by overexpression of DD and RIPK3, or the same overexpression including active dimerization of DD. Moreover, the tumors growing on the challenge site of the unvaccinated (PBS) mice were significantly larger than the tumors occurring on the mice receiving vaccines with necroptotic cells (Figure 3E), confirming that necroptotic cells induce a potent immune response in vivo.

To further examine the adaptive immune response to the anti-tumor vaccination achieved with the necroptotic DD_RIPK3 cells, we measured the cross-priming, proliferation, and cytokine release of cytotoxic T cells isolated from the draining inguinal lymph nodes of vaccinated mice (Figure 3F). We found that the draining lymph nodes of mice immunized with necroptotic DD_RIPK3 cells killed by doxy alone or by doxy and B/B contained tumor antigen-specific proliferating cytotoxic $CD8a^+$ T cells (Figures 3G and 3H), demonstrating the ability of necroptotic cells to activate the adaptive immune system in vivo. We also observed that tumor antigen-specific $CD8a^+$ T cells had statistically significant higher tetramer staining intensity in mice vaccinated with DD_RIPK3 necroptotic tumor cells compared with unvaccinated mice, as well as compared with mice that were immunized with F/T accidentally necrotic cells (Figure 3I). Interestingly, this cross-priming in vivo was absent or below the detection limit in mice vaccinated with accidentally necrotic cells, confirming the lower immunogenicity of F/T accidental necrotic cells. Correspondingly, vaccination of mice with DD_RIPK3 necroptotic cells also primed the immune cells for IFN-γ production in an ex vivo re-stimulation assay with an H2-L^d-restricted peptide (AH-1) (Huang et al., 1996) of both draining inguinal lymph nodes and spleens (Figures 3J and 3K). Note that the detection of tetramer staining is a subject of variation in our analysis (Figures 3G and 3I), probably reflecting the lack of sensitivity of such staining or differences in timing of the immune response in the individual mice, because mouse samples that are negative for one parameter do score positive for all other parameters examined.

DAMPs and Chemokines Are Secreted from Necroptotic Cells

One of the main characteristics of immunogenic apoptosis is the spatiotemporally coordinated emission of DAMPs such as ATP and HMGB1, which have a beneficial role in anticancer therapy owing to their interaction with the immune system (Apetoh et al., 2007; Garg et al., 2012b; Michaud et al., 2011). By mimicking in vitro the prophylactic vaccination setup, in which the dead cells are washed in PBS before injection into the mice, we observed that the DD_RIPK3 cells treated with doxy ± B/B continue to die up to 24 hr after being re-seeded in fresh medium without inducer and dimerizer (Figures S2A, S2B, and S2F). After re-seeding, the cells continued to release lactate dehydrogenase (LDH) and HMGB1 (Figures S2C and S2D). In addition,

(B) Representative dot plots (quantified in Figure 2D) showing the gating and percentage of $CD11c^+CD86^+MHC\text{-}II^+$ BMDCs in co-culture ratio 1:10 with necroptotic (doxy + B/B), untreated (UT) DD_RIPK3 cells, accidental necrotic F/T CT26 wild-type (WT) cells, or untreated (UT) CT26 WT cells.

(C) Representative dot plots (quantified in Figure 2E) showing the gating and percentage of $CD11c^+CD80^+MHC\text{-}II^+$ BMDCs in co-culture 1:10 with necroptotic (doxy + B/B), untreated (UT) DD_RIPK3 cells, accidental necrotic F/T, or untreated (UT) CT26 WT cells.

(D) Co-culture of BMDCs with necroptotic or accidental necrotic F/T cells in two different ratios (1:1 and 1:10). Percentage of $CD11c^+CD86^+MHC\text{-}II^+$ BMDCs expressed as the mean value + SEM of four independent experiments (in which three of the experiments included F/T cells).

(E) Co-culture of BMDCs with necroptotic and accidental necrotic F/T cells in two different ratios (1:1 and 1:10). Percentage of $CD11c^+CD80^+MHC\text{-}II^+$ cells expressed as the mean value + SEM of four independent experiments (in which three of the experiments included F/T cells). In Figures 2B–2E, BMDCs stimulated with lipopolysaccharide (LPS) served as a positive control.

Please cite this article in press as: Aaes et al., Vaccination with Necroptotic Cancer Cells Induces Efficient Anti-tumor Immunity, Cell Reports (2016), http://dx.doi.org/10.1016/j.celrep.2016.03.037

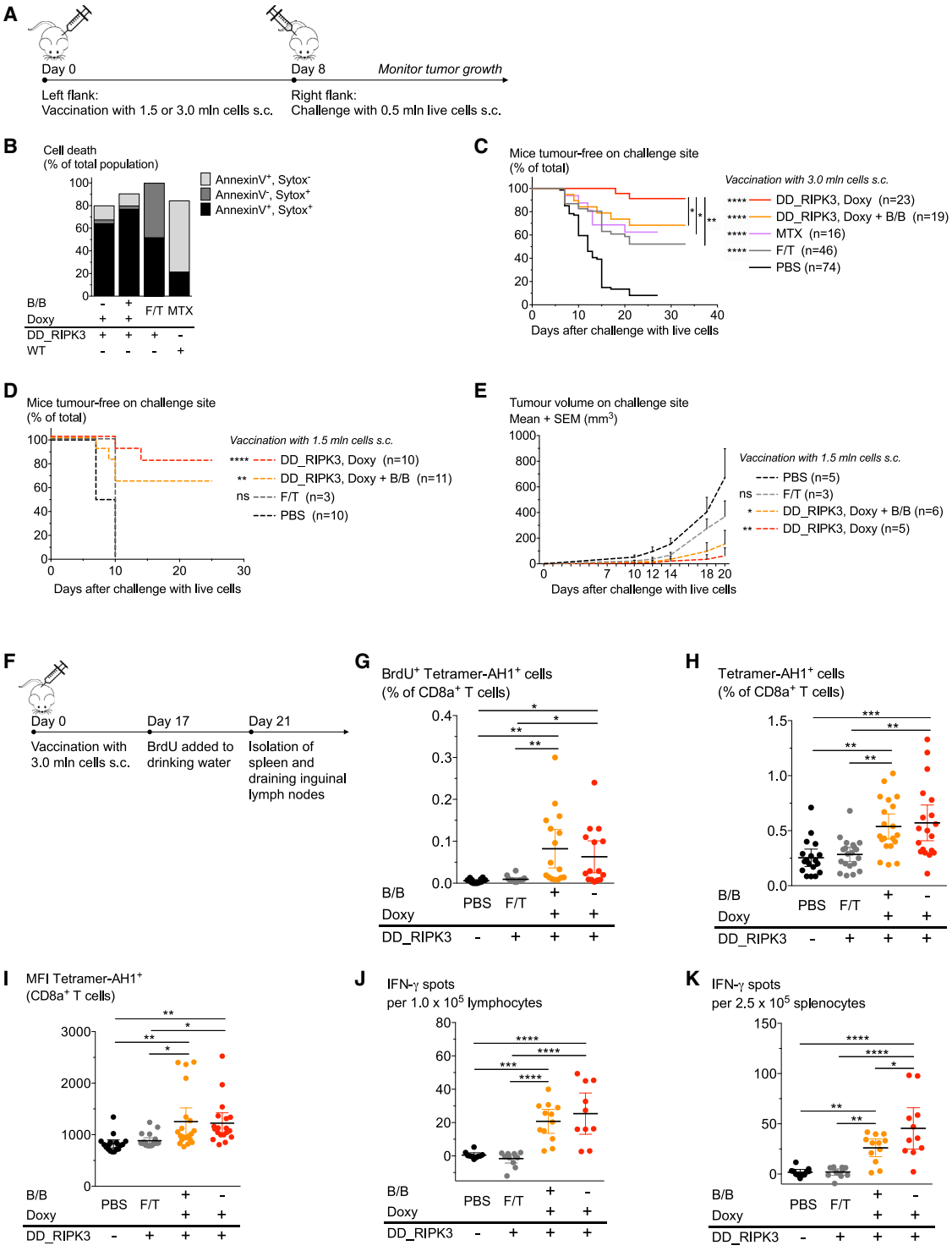

Figure 3. Necroptotic Cells Induce Anti-tumor Immunogenicity with Cross-Priming and Proliferation of CD8a$^+$ T Cells

(A) The prophylactic tumor vaccination model used in vivo in Figures 3C, 3D, and 4F.

(B) Cell death measured by flow cytometry of the cells used for immunization (representative results from one experiment) of the mice in Figure 3C. The cells used for immunization were stimulated (with doxycycline, mitoxantrone, or co-stimulated with doxycycline + B/B) and re-suspended in PBS before injection.

(C) Necroptosis induced by doxy or by doxy + B/B triggers an anti-tumor immune response when immunizing mice with 3.0 M cells. For a positive control, we vaccinated the mice with 3 M immunogenic apoptotic cells, which were killed by mitoxantrone (MTX) (Obeid et al., 2007a). Pool of eight independent experiments; n = total number of mice per group. The statistical difference from PBS is shown for each vaccination group or in-between groups as indicated by the vertical bars.

(legend continued on next page)

progressive secretion and accumulation of the chemokine CXCL1 was also observed in these cultures (Figure S2E). Consistent with the higher upregulation of Cxcl1 (Figure 4B), we also detect higher amounts of CXCL1 secreted upon co-stimulation of DD_RIPK3 cells with the B/B homodimerizer. CXCL1 is detected in the conditioned medium from only regulated necroptotic cells, and not in that of accidental necrotic (F/T) cells; whereas the passive release of e.g., ATP (Figure S2G) is detected in the conditioned medium of both regulated and accidental necrosis, as well as to a minor degree in that of untreated cells. The latter is probably due to spontaneous cell death caused by the over-growth of cells 24 hr after re-seeding.

One of the common prerequisites of immunogenicity triggered by most IA-inducing stimuli is the induction of PERK-mediated endoplasmic reticulum (ER) stress (Krysko et al., 2012), which leads to calreticulin exposure on the cell surface, and thereby acts as an ''eat-me'' signal (Garg et al., 2012b; Panaretakis et al., 2009). Yet, we found that the necroptotic tumor cells do not show any pronounced features of ER stress (Figure S3), suggesting that in our DD_RIPK3 cells the immunogenicity of necroptosis is mainly disengaged from any ER stress.

Role of NF-κB Activation in Immunogenicity of Necroptosis

Cytokine secretion by dying tumor cells has been proven to enhance the anti-tumor immunity and thereby also the clearance of tumor cells (Jinushi et al., 2008). Recently, it has been shown that NF-κB signaling in NIH 3T3 fibroblasts undergoing necroptosis is a requirement for efficient cross-priming of $CD8^+$ T cells (Yatim et al., 2015). Therefore, we also examined the status of NF-κB activation in CT26 cells undergoing necroptosis. We only observed clear NF-κB activation when necroptosis was associated with induced DD dimerization as shown by phosphorylation and concomitant degradation of IκBα (Figure 4A). These results correlate with those of an RT-qPCR expression analysis focusing on a panel of NF-κB-regulated inflammatory genes, in which we observed a higher upregulation of cytokine/chemokine-encoding genes when necroptosis is induced by doxy and B/B rather than by doxy only (Figure 4B).

To better distinguish between the contribution of RIPK3 overexpression with and without DD dimerization to NF-κB activation, we generated two additional Tet-On inducible CT26 cell lines (Figure 4C; Table 1), expressing RIPK3 or a combination of RIPK3 with dimerizable FADD (FADD_RIPK3). The combined expression and dimerization of FADD in the presence of RIPK3 (Figure 4D; Movie S3), or the mere overexpression of RIPK3 (Figure 4D; Movie S4), led to necroptotic cell death as observed by the absence of DEVD activity (Figure 4D), phosphorylation of MLKL Ser345 (Figure 4E), oncosis morphology and plasma membrane permeabilization (Movies S3 and S4). Notably, both additional inducible necroptosis cell lines (FADD_RIPK3; RIPK3) were also immunogenic when used to immunize immunocompetent mice in the in vivo prophylactic tumor vaccination model (Figure 4F). Moreover, the immunogenicity of these two CT26 cell lines (FADD_RIPK3; RIPK3) used in the prophylactic tumor vaccination model (in the experiment shown in Figure 4F) also elicited an efficient anti-tumor immune response, because the tumors growing on the challenge site of these mice were significantly smaller than those on the unvaccinated mice (Figure 4G). However, we clearly observed NF-κB activation (phosphorylation and concomitant degradation of IκBα) only in the cell line where necroptosis was associated with the dimerization of FADD (Figure 4H), again suggesting that the extent of NF-κB activation is uncorrelated with the observed immunogenicity induced by necroptotic cells in our model.

Although it has been reported that RIPK3 can mediate NLRP3 inflammasome activation and IL-1β activation (Kang et al., 2013; Vince et al., 2012), we could not detect IL-1β, neither at mRNA level nor at protein level in necroptotic DD_RIPK3 cells (induced with doxy + B/B) and their supernatant respectively (data not shown), thereby excluding the role of IL-1β in immunogenicity in our system.

DISCUSSION

Our results demonstrate that cancerous cells undergoing necroptosis can be immunogenic. This immunogenicity was shown in vitro, where upon co-culture with BMDCs, the necroptotic cells were phagocytized and resulted in the phenotypic

The one-star difference between the two DD_RIPK3 groups (±B/B) corresponds to a p value of 0.0492. The difference between DD_RIPK3 doxy and MTX has a p value of 0.0205.

(D) Immunization with only 1.5 M necroptotic cells is highly efficient. Pool of two independent experiments (immunization with F/T was done once); n = total number of mice per group. The statistical difference from PBS is shown for each vaccination group.

(E) The size of the tumors growing on the challenge site of the mice that were used in the prophylactic tumor vaccination experiments. Data represent one of the two experiments shown in Figure 3D. The statistical difference from PBS is shown for each vaccination group.

(F) The experimental setup preceding the analysis of T cell proliferation, cross-priming, and IFN-γ production of BALB/c mice immunized with 3.0 M cells (cf. Figures 3G–3K). Each dot in Figures 3G–3K represents one mouse, and each error bar represents the 95% confidence interval (CI).

(G) The proportion of proliferating ($BrdU^+$) tumor antigen-specific ($Tetramer\text{-}AH1^+$) $CD8a^+$ T cells derived from the inguinal draining lymph nodes of immunized mice (see labels on the x axis). Mean value with 95% CI of four independent experiments; n = 14–16 mice per vaccination group.

(H) The proportion of tumor antigen-specific ($Tetramer\text{-}AH1^+$) $CD8a^+$ T cells derived from the inguinal draining lymph nodes of immunized mice (see labels on the x axis). Mean value with 95% CI of five independent experiments; n = 18–20 mice per vaccination group.

(I) The median fluorescence intensity (MFI) of tumor antigen-specific ($Tetramer\text{-}AH1^+$) $CD8a^+$ T cells from the inguinal draining lymph nodes of immunized mice (see labels on the x axis). Mean value with 95% CI of five independent experiments; n = 18–20 mice per vaccination group.

(J) IFN-γ ELISpot assay using the inguinal draining lymph nodes of immunized mice (see labels on x axis). Mean value with 95% CI of triplicates from three independent experiments; n = 11–12 mice per vaccination group.

(K) IFN-γ ELISpot assay using the spleens of immunized mice (see labels on x axis). Mean value with 95% CI of triplicates from three independent experiments; n = 11–12 mice per vaccination group. No statistically significant difference was measured between PBS and F/T in Figures 3G–3K or between doxy and doxy + B/B in Figures 3G–3J.

Please cite this article in press as: Aaes et al., Vaccination with Necroptotic Cancer Cells Induces Efficient Anti-tumor Immunity, Cell Reports (2016), http://dx.doi.org/10.1016/j.celrep.2016.03.037

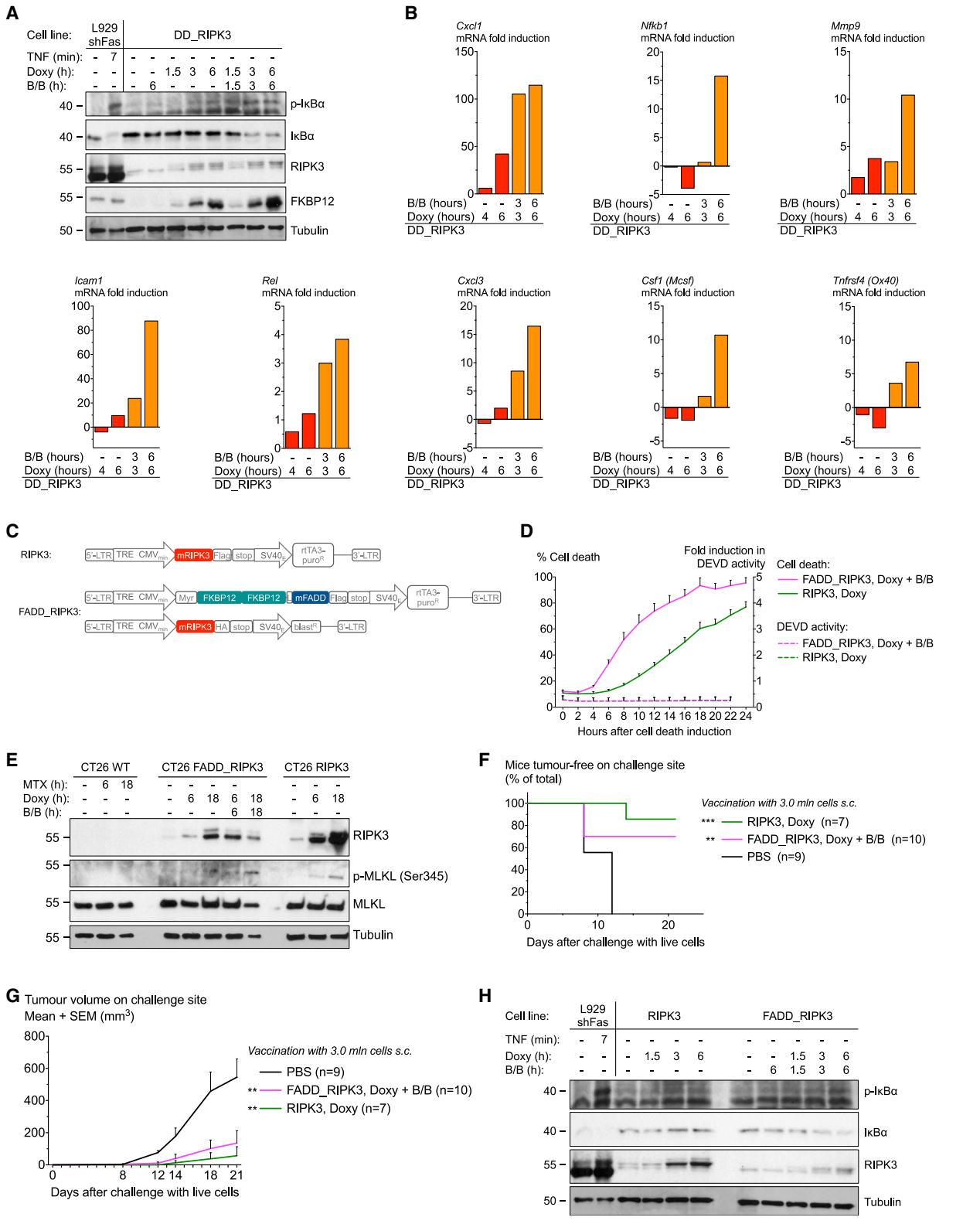

Figure 4. Role of NF-κB Activation in Immunogenicity of Necroptosis

(A) Western blot shows NF-κB activation (phosphorylation of IκBα [p-IκBα] and its subsequent degradation [IκBα]) upon stimulation with doxy + B/B, but less when stimulating with doxy only. Representative blot of three independent experiments.

(legend continued on next page)

maturation of BMDCs, as well as in vivo, where necroptotic cells served as potent immunizers in a prophylactic tumor vaccination model. Necroptotic cells induced effective cross-priming of cytotoxic $CD8a^+$ T cells in vivo, and they mediated a strong CT26 tumor antigen-specific production of IFN-γ ex vivo. In our experiments, the immunogenicity of necroptotic cells does not seem to correlate with the level of NF-κB activation in vitro. Thus, taken together, necroptotic cancer cells appear to be potent inducers of an adaptive immune response and mediate efficient anti-tumor immunity.

Several models of necroptosis in tumor cells have been described, and they are mainly based on ligand-dependent activation of certain members of the TNFR (e.g., TNF) and TLR families (e.g., LPS and PolyI:C) (Krysko et al., 2006; Takemura et al., 2015; Vanlangenakker et al., 2011). However, when used in vivo, these necroptosis-inducing ligands may also target the host immune system and therefore do not allow evaluation of the immune response resulting uniquely from necroptosis induction. To circumvent this ligand transfer in our study, we developed a ligand-free tetracycline-inducible gene expression system, which enables us to conditionally induce RIPK3-dependent necroptosis in syngeneic murine colon carcinoma CT26 cells. This cell line has already been widely used to characterize the ability of anti-cancer therapies to induce immunogenic apoptosis (Casares et al., 2005; Garg et al., 2012b; Michaud et al., 2011; Obeid et al., 2007b). RIPK3 was the necroptosis-inducer of choice, given that it is required for activation of the necroptotic pathway (Cho et al., 2009; Zhang et al., 2009). We also expressed the dimerizable death domain (DD) of FADD as a platform favoring necroptosis (Vanden Berghe et al., 2004). In this study, we also provide evidence that at low cell numbers used for vaccination, the immunogenicity of necrotic cancer cells is more efficient when the cells undergo a cell death program rather than die by F/T accidental necrosis. F/T accidental necrotic cells are immunogenic only when used in high numbers for vaccination (3.0 M cells per mouse), but yet they neither induce cross-priming of $CD8a^+$ T cells nor do they give rise to tumor antigen-specific IFN-γ production.

Our data are in line with a recently published study (Yatim et al., 2015), in which it is shown that necroptosis induced by overexpression and dimerization of RIPK3, but not accidental necrotic cells, induces the efficient cross-priming of $CD8a^+$ T cells. Together, the data of Yatim et al. (2015) (in NIH 3T3 fibroblast cells) and our results (in CT26 colon carcinoma cells) strongly suggest that necroptosis is immunogenic in a cell-type-independent manner. Additionally, our findings also suggest that, as opposed to IA-induced (Panaretakis et al., 2009) and hypericin-based photodynamic therapy (Garg et al., 2012b), the immunogenic necroptosis induced in our system is apparently not associated with any pronounced ER stress or PERK activation. Nevertheless, the necroptotic cells are strongly immunogenic. It is therefore conceivable that other mechanisms than merely ER stress or PERK activation must be a requisition for an efficient anti-tumor response.

It has been shown that dimerization of RIPK3 in fibroblasts leads to NF-κB activation in necroptotic cells, and interestingly it was demonstrated that blocking this NF-κB signaling reduced the cross-priming efficiency of $CD8^+$ T cells (Yatim et al., 2015). However, in our study we observed that immunogenicity of necroptotic cancerous cells does not correlate with the activation status of NF-κB signaling measured in vitro. Prominent NF-κB activation appeared, in our system, to be dependent on the active dimerization of full-length FADD or of the FADD death domains (DD). Concomitantly, the overexpression of RIPK3, together with dimerization of DD, resulted in an upregulation of several genes, which are transcriptionally induced by NF-κB, as opposed to necroptosis induced without DD dimerization in the same cell line. Whether this phenomenon is applicable to other cell death-inducing systems with/without FADD or DD dimerization is a subject for future investigation. Importantly, a main difference between the findings of Yatim et al. (2015) and those of our study is the way the dying cells were administered as vaccine: Yatim et al. (2015) injected treated living fibroblasts (MEFs and NIH 3T3 cells), which further die in vivo over a longer period of time. In contrast, we injected PBS-washed dead cancerous cells. It is conceivable that our bolus injection of dead cells requires fewer NF-κB-dependent factors because enough DAMPs or other signals are present to overrule the NF-κB dependency. This diverting feature is of great interest and will be further investigated in our future experiments.

(B) qRT-PCR data shows the upregulation of NF-κB-regulated inflammation-associated genes during necroptosis induced by doxy + B/B or by doxy (average normalized relative quantities, fold induction compared to untreated DD_RIPK3 cells). Presented values are the means of triplicate samples from one experiment (or from two independent experiments for 4-h doxy only).

(C) The Tet-On-inducible constructs introduced into the CT26 cells, which were used in Figures 4D–4H.

(D) Cell death progression measured by SYTOX Green fluorescence and caspase activity by DEVD-AMC cleavage. Overexpression and dimerization of FADD, along with the overexpression of RIPK3, or by overexpression of RIPK3 induces cell death with no DEVD activity. Pool of three independent experiments.

(E) Western blot shows phosphorylation of MLKL (p-MLKL) on Ser345 on induction of FADD_RIPK3 cells with doxy + B/B or RIPK3 cells with doxy alone. During apoptosis induction by mitoxantrone (MTX) in WT cells, we detect no RIPK3 or p-MLKL expression. Representative blot from one of two independent experiments.

(F) In the prophylactic tumor vaccination model, necroptosis induced by the overexpression of RIPK3 or by the overexpression and dimerization of FADD_RIPK3 is immunogenic. The mice were immunized with 3.0 M dead cells. Pool of two independent experiments; n = the total number of mice per group. The statistical difference from PBS is shown for each vaccination group.

(G) The size of the tumors growing on the challenge site of the mice that were used in the prophylactic tumor vaccination experiments. Data represent the pool of the two experiments shown in Figure 4F. The statistical difference from PBS is shown for each vaccination group.

(H) Western blot analysis shows NF-κB activation during necroptosis mainly under conditions in which FADD is dimerized. The faint RIPK3 bands observed in the unstimulated RIPK3 (lane 3) and RIPK3_FADD (lane 8) cells is due to a slight leakiness of the RIPK3 construct. Representative blot of one of two independent experiments.

See also Movies S3 and S4.

Please cite this article in press as: Aaes et al., Vaccination with Necroptotic Cancer Cells Induces Efficient Anti-tumor Immunity, Cell Reports (2016), http://dx.doi.org/10.1016/j.celrep.2016.03.037

Considering that RIPK3 expression is lost in many cancer cell lines (He et al., 2009), as well as in primary human cancers, such as breast cancer (Koo et al., 2015) and acute myeloid leukemia (Nugues et al., 2014), a strategy might indeed be to restore RIPK3 expression in the cancer cells through the application of hypomethylating agents (Koo et al., 2015), or via (oncolytic) virus-mediated expression of RIPK3. One way to induce RIPK3-dependent necrotic cell death is by 5-aminolevulinic acid-based photodynamic therapy (Fulda, 2014), and it may therefore be a possible mode of cell death induction in apoptosis-resistant cancers.

To date, the observation of immunogenic dying cancer cells is restricted to immunogenic apoptosis (Casares et al., 2005; Garg et al., 2012a, 2012b; Ghiringhelli et al., 2009; Michaud et al., 2011; Obeid et al., 2007a). Our study indicates that (1) necroptotic cancerous cells release DAMPs (ATP and HMGB1), induce maturation of dendritic cells and production of IFN-γ by T cells, and mediate anti-tumor immunity, (2) induction of a regulated cell death program is required for efficient immunogenicity of dead cells, and (3) immunogenicity of necroptosis does not correlate with the extent of NF-κB activation status. Our finding that necroptotic tumor cells are strongly immunogenic broadens the current concept of immunogenic cell death. In a clinical setting, this will become beneficial for patients with apoptosis-resistant cancers, providing that pharmacological strategies are redesigned to compensate for defective cell death signaling by inducing alternative immunogenic cell modalities, such as necroptosis.

EXPERIMENTAL PROCEDURES

Cell Lines and Cell Culture

The murine colon carcinoma CT26 cells and its derivates were cultured in DMEM (GIBCO), supplemented with 10% heat-inactivated fetal calf serum (FCS) (Life Technologies), L-glutamine (0.03%), and sodium pyruvate (0.4 mM), all LPS-free products. Cells were cultured at 37°C in the presence of 5% CO_2 and were tested for the absence of mycoplasma contamination on a regular basis.

The FADD_RIPK3 cell line was first obtained by transduction of CT26 cells with pDG2-flag-rtTA3-puro-Myr-2FKBP12-L-FADD plasmid. This is a tetracycline-inducible derivative of pLenti6 (Life Technologies) also containing a puromycin selection marker, in which the coding sequence for a myristoylation (Myr)-targeting peptide, two tandem repeats of FKBP12 (Clontech), a short linker peptide (L, GSGGGS), and the full-length murine cDNA of FADD (Open Biosystems, BC021400) were cloned. Upon lentiviral transduction, the stably transduced cells were selected with 9 μg/ml puromycin and transduced again with a tetracycline-inducible pDG1-HA-blast-RIPK3 in which mouse cDNA of RIPK3 was cloned. pDG1 RIPK3-HA-blast contains a blasticidin selection marker and the influenza HA epitope from ARIAD. Then the stably transduced cells were selected with 9 μg/ml puromycin and 7 μg/ml blasticidin, and clones were obtained by limited dilution. Necroptosis was induced by 1 μg/ml doxycycline and 10 nM of B/B homodimerizer (Clontech).

The DD_RIPK3 cell line was first generated by transduction of CT26 cells with pDG2-flag-rtTA3-puro-Myr-2FKBP12-L-DD plasmid. This plasmid is tetracycline inducible and contains the coding sequence for a Myr-targeting peptide, two tandem repeats of FKBP12 (Clontech), a short linker peptide (L, GSGGGS), and the death domain (amino acids 80–205) of the murine FADD (Open Biosystems, BC021400). Upon lentiviral transduction, the stably transduced cells were selected with 9 μg/ml puromycin and transduced again with a tetracycline-inducible pDG2 RIPK3-HA-blast in which mouse cDNA of RIPK3 was cloned. pDG1 RIPK3-HA-blast contains a blasticidin selection marker and the influenza HA epitope from ARIAD. Then the stably transduced cells were selected with 9 μg/ml puromycin and 7 μg/ml blasticidin, and clones were obtained by limited dilution. Necroptosis was induced by 1 μg/ml doxycycline and 10 nM of B/B homodimerizer or by induction with 1 μg/ml doxycycline only.

Transducing CT26 cells with pDG2-flag-rtTA3-puro-mRIPK3 generated the RIPK3-overexpressing cells. Stably transduced cells were selected with 9 μg/ml puromycin, and clones were obtained by limited dilution. Necroptosis was induced by stimulation with 1 μg/ml doxycycline.

Cell Death Assay on FLUOstar OMEGA

Cell death was analyzed on a FLUOstar OMEGA (BMG Labtech). 6,000 to 10,000 cells were seeded in a transparent 96-well plate. 2 μM SYTOX Green nucleic acid stain (Molecular Probes, S7020) and 33 μM Ac-DEVD-AMC (Peptanova, 3171-V) were added to the cells, and the cells were then stimulated with doxycycline or doxycycline + B/B as described above.

Maximal cell death was obtained by treatment with Triton X-100 (0.05%). This allowed the expression of cell death as a percent of the control of maximal SYTOX Green fluorescence (excitation 485 nm, emission 520 nm). If the executor caspases-3/-7 are activated during cell death, they cleave Ac-DEVD-AMC only upon plasma membrane rupture, resulting in the release of fluorescent 7-amino-4-methylcoumarin (AMC) (excitation 355 nm, emission 460 nm). The DEVD activity is expressed as fold induction compared to the maximal fluorescence intensity value.

Cell Death Assay by Flow Cytometry

The cells were washed in Annexin V binding buffer (BD Bioscences, 556454), followed by a staining with SYTOX Blue Nucleic Acid Stain (Molecular Probes, S11348) and APC Annexin V (BD Biosciences, 550474) or Annexin V, Alexa Fluor 488 conjugate (Molecular Probes, A13201) and run on a BD FACSVerse flow cytometer. The data were analyzed using FlowJo software.

Small Interfering RNA-Mediated Knockdown

DD_RIPK3 cells were transiently transfected with Dharmacon small interfering RNAs against MLKL (GenBank: XM_924585) GAGAUCCAGUUCAACGAUA, RIPK1 (GenBank: NM_009068) UCACCAAUGUUGCAGGAUA, or nonspecific (D-001810-10-20). 3,000 cells were seeded in 96-well (for FLUOstar), or 24-well plates (for western blotting), and were transfected in accordance with the manufacturer's protocols by using Dharmafect-1 transfection reagent (Thermo Fisher Scientific, T-2001-03). The cell death in DD_RIPK3 cells was induced by doxycycline or doxycycline + B/B, and the percentage of cell death and caspase-3/7 activity were determined as described above. The efficiency of knockdown was analyzed by western blotting.

Live-Cell Imaging

Cells were seeded in an eight-well chamber (iBidi), with 15,000 cells per well in 200 μl complete growth medium. Cell death was induced just before imaging, and cell death was monitored by SYTOX Green (10 nM, Molecular Probes). Live-cell imaging was performed on a Leica Sp5 AOBS confocal microscope (Leica), using a 40× HCX PL Apo UV 1.25 na oil objective. Cells were imaged for bright field and SYTOX Green using the 488 line of a Multi-line Argon Laser. Images were acquired in a sequential mode. Images were captured in three frames per well every 20 min, and the pinhole was opened to 2 AU to prevent phototoxicity and photobleaching; likewise, the scanner was set at a speed of 700 Hz. Different focal planes were set at 1-μm intervals. From each image stack, maximum intensity projections for SYTOX Green and montages of the multi-tiff time series and two-channel overlays were made using ImageJ 1.49 m, a public domain imaging software.

Western Blot Analysis

Samples were lysed in Laemmli buffer containing 50 mM Tris HCl (pH 6.8), 2% SDS, and 10% glycerol. The protein concentration for each sample was determined using a NanoDrop 1000 spectrophotometer in accordance with the manufacturer's recommendations. The proteins were separated by SDS-PAGE and transferred to nitrocellulose membranes.

Western blotting was performed with anti-FKBP12 (Thermo Scientific PA1-026A), anti-RIPK3 (Sigma Aldrich, R4277), anti-Caspase 8 (Abnova, MAB3429), anti-Cleaved caspase-8 (Cell Signaling Technology, 9429),

anti-Caspase 3 (Cell Signaling Technology, 9662), anti-Cleaved PARP (Cell Signaling Technology, 9544), anti-actin (MP Biomedicals, 69100), anti-phospho-IκB-α (Cell Signaling Technology, 9246), anti-IκB-α (Santa Cruz Biotechnology, sc-371), anti-RIPK3 (ProSci, 2283), anti-tubulin HRP (Abcam, ab21058), anti-FADD (Santa Cruz, sc-6036), anti-RIPK1 (BD Biosciences, 610459), anti-HA (Covance, MMS-101R), anti-MLKL (Millipore, MABC604), anti-phospho-MLKL S345 (Abcam, ab196436), anti-phospho-PERK (Cell Signaling Technology, 3179S), anti-PERK (Cell Signaling Technology, 3192S), anti-phospho-eIF2α (Cell Signaling Technology, 3597S), anti-eIF2α (Cell Signaling Technology, 2103S), anti-CHOP (Cell Signaling Technology, 2895S), anti-BiP (Cell Signaling Technology, 3183S), and anti-XBP1 (Abcam, ab37152).

Amersham ECL HRP-linked sheep anti-mouse immunoglobulin G (IgG) (NA931), donkey anti-rabbit IgG (NA934), or goat anti-rat IgG (NA935) secondary antibodies were from GE Healthcare Life Sciences. After incubation with the appropriate secondary antibodies conjugated to horseradish peroxidase, blots were revealed using ECL western blotting substrate (Pierce, 32106), or Western Lightning plus-ECL (PerkinElmer, NEL105001EA).

Immunoprecipitation

1.25×10^6 CT26 DD_RIPK3 cells were seeded per 10-cm petri dish. The next day, the cells were stimulated with doxycycline, doxycycline + B/B added simultaneously, or doxycycline + B/B added for the last half an hour. After treatment with the indicated triggers, the cells were washed with PBS and lysed in NP-40 lysis buffer (150 mM NaCl, 1% NP-40, 10% glycerol, and 10 mM Tris-HCl [pH, 8]), supplemented with cOmplete, EDTA-free protease inhibitor cocktail tablets (Roche, 11873580001), and PhosSTOP phosphatase inhibitor cocktail tablets (Roche, 04906837001). Immunoprecipitation was done overnight using protein G-coupled anti-FADD (Santa Cruz, sc-6036), protein A-coupled anti-Caspase-8 (homemade antibody), or protein A-coupled anti-RIPK3 (Pro-Sci, 2283). After all immunoprecipitations, the beads were washed three times in NP-40 lysis buffer, and the immunoprecipitated proteins were eluted by adding 60 μl of 2× Laemmli buffer to the beads. Complexes were subsequently analyzed by immunoblotting (20 μl protein loaded per lane).

LDH, ATP, HMGB1, and CXCL1 Release after Cell Reseeding

DD_RIPK3 cells were seeded in 96-well plates (for LDH release assay) and in 10-cm petri dishes (for ATP, HMGB1, and CXCL1 release assays), left to adhere for 4 hr, and then treated with the indicated drugs for another 18 hr. Supernatants and cells were collected from all conditions. The remaining cells were washed once in PBS and reseeded in 24-well plates or in a 96-well plate (for the LDH assay). After the indicated time points, supernatant was collected and cleared from dying tumor cells by centrifugation (1,500 rpm, for 5 min; except for the ATP assay, as centrifugation can stimulate release, independently from stimulation and cell death). The supernatant was either used immediately for LDH cytotoxicity assay (Cayman Chemical) and ATP quantification (ATP Bioluminescent Assay Kit, Sigma-Aldrich) or frozen at −20°C for later use for HMGB1 quantification by an ELISA kit (IBL-Hamburg), and CXCL1 quantification using a bead-based multiplex immunoassay (ProcartaPlex, eBioscience). All assays were performed in accordance with the respective manufacturers' instructions. LDH and HMGB1 were quantified using the iMARK microplate absorbance reader (Bio-Rad), and for HMGB1, the data were analyzed with a Four Parameter Logistic Curve Fit (MyAssays.com). ATP was measured with the GloMax 96-microplate luminometer (Promega). CXCL1 release was measured with Bio-Plex 200 Systems (Bio-Rad) and analyzed with the Bio-Plex Manager software.

Generation of Mouse BMDCs

BMDCs were differentiated from the femurs and tibias of 7-week-old BALB/c mice for 8 days using RPMI 1640 medium (GIBCO), supplemented with 5% heat-inactivated fetal calf serum, L-glutamine (0.03%), sodium pyruvate (0.4 mM), 2-mercapthoethanol (50 μM), and mGM-CSF (20 ng/ml). Fresh culture medium was added on day 3, and on day 6 the medium was refreshed.

Phagocytosis Assay

The target cells, CT26 DD_RIPK3 cells, were labeled with 1 μM CellTracker Green CMFDA (Molecular Probes, C7025) for 30 min and were then either left untreated or induced to cell death by stimulation with doxycycline for 18 hr. The cells were collected, washed, and co-cultured with BMDCs in a ratio 1:1 for 2 hr. Next, the co-cultured cells were harvested, incubated with a mouse Fc block (BD PharMingen, 553142), immunostained with APC-anti-CD11c (BD PharMingen, 550261), and, finally, analyzed by flow cytometry on the BD FACSVerse. Analysis was performed using FlowJo (v.10.0.8) software. True uptake of CMFDA-labeled dead cell material by BMDCs was determined using a gating strategy that allows analysis of only single cells and was determined as $CD11c^+CMFDA^+$ double-positive cells. Cell death of the CT26 cells was determined by flow cytometry as described above and was analyzed concurrently with the phagocytosis assay samples.

Analysis of BMDCs Surface-Marker Expression

Cell death was induced in the DD_RIPK3 cells on the addition of doxycycline and B/B homodimerizer for 18 hr. The dead DD_RIPK3 cells were collected, washed in RPMI culture medium, and co-cultured with 50,000 BMDCs in two different ratios: 1:1 and 1:10. In parallel, CT26 WT cells were subjected three times to freeze-thaw cycles and co-cultured with BMDCs in the same ratios and cell numbers as the DD_RIPK3 cells. Co-culture was performed for 18 hr at 37°C in six-well plates with 2.5 ml RPMI culture medium.

Control BMDCs were left untreated or stimulated with 100 ng/ml LPS (Sigma Aldrich, L2630). After 18 hr co-culture, all cells were collected, spun down (400 × *g*, for 6 min, 4°C), and washed once in PBS (GIBCO DPBS, Life Technologies, 14190-094) + 0.5% FCS. Dead cells were excluded from the flow cytometry analysis by staining with SYTOX Blue (Molecular Probes, S11348). Maturation of BMDCs was analyzed by immunostaining using APC-anti-CD11c (BD PharMingen, 550261), FITC-anti-MHC class II (eBioscience, 11-5321), PE-Cy7-anti-CD86 (BD PharMingen, 560582), PerCP-Cy5.5-anti-CD80 (Molecular Probes, A14895), and mouse Fc block (BD PharMingen, 553142).

Gating strategy: Single cells were obtained by gating on FSC-A versus FSC-H, followed by SSC-A versus SSC-H. Dead cells were excluded by SYTOX Blue. Mature BMDCs cells were identified as a percent of $CD11c^+MHCII^+CD86^+$ and $CD11c^+MHCII^+CD80^+$. All samples were acquired on the BD FACSVerse flow cytometer and analyzed with FlowJo 10.0.8 software.

Mice

Female BALB/c mice (6–7 weeks old) were purchased from Harlan Laboratories (Netherlands) or from Charles River Laboratories (France) and were housed in specific pathogen-free (SPF) conditions. All experiments were performed in accordance with the guidelines of the local Ethics Committee of Ghent University.

In Vivo Prophylactic Tumor Vaccination

CT26 cells were seeded on 15-cm petri dishes, and cell death was induced in vitro, either via the inducible systems for 18–24 hr or by incubating the cells with 2 μM mitoxantrone (Sigma, M6545) for 24 hr. After cell death induction, the cells were collected, washed once in PBS (GIBCO DPBS, Life Technologies, 14190-094), and re-suspended in the desired concentration in PBS. Mice were inoculated subcutaneously with 3×10^6 or 1.5×10^6 dying CT26 cells or with PBS on the left flank side. Accidental necrosis was induced by subjecting the CT26 cells, already resuspended in the desired PBS volume, three times to freeze-thaw cycles (dry ice/37°C). On day 8 after vaccination, the mice were challenged subcutaneously (s.c.) on the opposite flank with 5×10^5 live CT26 cells. Tumor growth on the challenge site was evaluated using an electronic caliper for up to 4 weeks after the challenge. Mice were sacrificed when tumors became necrotic or exceeded 2,000 mm^3.

Analysis of T Cell Cross-Priming and Proliferation

Mice were injected s.c. with 3×10^6 dying CT26 DD_RIPK3 cells or PBS at the tail base, which enabled a clear isolation of the draining inguinal lymph nodes. After 17 days, 0.8 mg/ml bromodeoxyuridine (BrdU, Sigma-Aldrich, B5002) was added to the drinking water. 4 days later, thus 3 weeks after immunization, the mice were sacrificed, and the spleens and inguinal draining lymph nodes were isolated. The spleens were treated twice with ACK Lysing Buffer (Lonza, 10-548E), and along with the lymph node samples, the cells were spun down (400 × *g*, for 7 min, at 4°C), before they were resuspended in PBS (GIBCO DPBS, Life Technologies, 14190-094). The cells were stained with

MHC Dextramer (H-2 Ld/SPSYVYHQF-PE, Immudex, JG3294-PE), followed by anti-CD4 (BD Pharmingen, 557307), anti-CD8a (BD Pharmingen, 553036), anti-CD3e (BD Pharmingen, 558214), anti-CD19 (eBiosciences, 56-0193-82), mouse Fc block (BD Pharmingen, 553142), and LIVE/DEAD Fixable Aqua Dead Cell Stain Kit (Molecular Probes, L34957).

Fixation and BrdU staining was performed in accordance with the manufacturer's protocol (eBioscience, 8817-6600-42). Compensation was made with the use of UltraComp eBeads (eBioscience, 01-2222-42). Flow cytometry acquisition was performed with the BD LSR II HTS flow cytometer (BD Biosciences). Data were analyzed using FlowJo (v.10.0.8) software.

Ex Vivo Restimulation of Lymphocytes and IFN-γ ELISpot Assay

Spleens and inguinal draining lymph nodes were isolated from mice 3 weeks after immunization (see Analysis of T Cell Cross-Priming and Proliferation). Following lysis of erythrocytes, 1.0×10^5 lymph node cells from the draining lymph nodes or 2.5×10^5 splenocytes were seeded per well on an IFN-γ capture antibody-coated 96-well polyvinylidene fluoride-bottomed plate (Millipore, MSIPS4510), and the cells were restimulated for 24 hr with 5 μg/ml of AH-1 peptide (SPSYVYHQF, tebu-bio, AS-64798); stimulation with 4 μg/ml concanavalin A type IV served as a positive control (Sigma-Aldrich, C2010). The murine IFN-γ ELISpot assay was performed in accordance with the manufacturer's instructions (Diaclone, 862.031.010). Spots were counted using an A.EL.VIS 4 Plate ELISPOT-Reader (v.2.1) and quantified with the A.EL.VIS Eli.Analyze software. The presented values (each dot) are the mean values of triplicate samples of AH-1 peptide-stimulated cells with background RPMI only stimulation subtracted from one mouse. The overall mean (black horizontal bar) and 95% CI (error bars) for each immunization is calculated for all of the mice from the three independent experiments.

qRT-PCR Analysis of Cytokine Expression

5×10^5 CT26 DD_RIPK3 cells were seeded in 6-cm dishes in 3 ml complete growth medium and were left untreated or stimulated with doxycycline or doxycycline + B/B for two different time points. RNA was isolated using the RNeasy Plus Mini Kit in accordance with the manufacturer's instructions (QIAGEN, 74134). Cell death was analyzed in parallel by flow cytometry. RNA concentration was measured on the NanoDrop 1000 spectrophotometer, followed by RNA quality assessment using Agilent RNA 6000 Nano Reagents and Nano Chips (Agilent Technologies, 5067-1511) and analyzed with the Agilent 2100 Bioanalyzer (Agilent Technologies). cDNA synthesis was performed with the iScript cDNA Synthesis Kit (Bio-Rad 170-8891), and gene expression was assessed with gene specific primers using Sensifast SYBR No-Rox kit (Bioline BIO-98020) on a LightCycler 480 instrument (Roche). Data were analyzed with qbase+ (Biogazelle) generating normalized relative quantities. The results shown represent the fold increase compared with the values obtained with the unstimulated DD_RIPK3 cells.

Statistical Analysis

Statistical analysis was performed in GraphPad Prism (v.6.0). The phagocytosis assay was analyzed by a Mann-Whitney non-parametric t test. The BMDCs activation and maturation assay was analyzed using a two-way ANOVA test. Kaplan-Meier survival curves showed the time line for tumor occurrence and were analyzed by the log-rank Mantel-Cox test. Differences in tumor volume on the mice in the vaccination experiments were analyzed with a two-way ANOVA with Tukey's multiple comparisons test. The T cell proliferation and cross-priming experiments and the IFN-γ ELISpot assays were all analyzed with an ordinary one-way ANOVA with Tukey's multiple comparisons test. The DAMPs measurements (ATP and HMGB1) were analyzed using a Mann-Whitney non-parametric t test. The difference in therapeutic tumor treatment was calculated using two-way ANOVA. *p value < 0.05, **p value < 0.01, ***p value < 0.001, ****p value < 0.0001. No exclusion criteria were used.

SUPPLEMENTAL INFORMATION

Supplemental Information includes Supplemental Experimental Procedures, three figures, and four movies and can be found with this article online at http://dx.doi.org/10.1016/j.celrep.2016.03.037.

AUTHOR CONTRIBUTIONS

P.V. and D.V.K. conceived of and designed the project. T.L.A., A.K., T.D., L.H., I.D., B.W., J.T., M.J.M.B., and A.D.G. performed the experiments. D.V.K., M.J.M.B., W.D., B.D., P.A., and S.D. supervised the experiments. T.L.A., A.K., P.V., and D.V.K. participated in manuscript preparation. D.V.K., P.V., M.J.M.B., P.D., W.D., B.D., P.A., J.G., and L.L. participated in designing the experiments. All authors discussed and reviewed the manuscript.

ACKNOWLEDGMENTS

This is a Cancer Research Institute Ghent paper (CRIG). We thank the Bio Imaging Core of Inflammation Research Center (VIB) and, in particular, Ms. Amanda Goncalves for her help with making the time-lapse movies. We thank Mrs. Susanne Løve Aaes-Jørgensen and Dr. Amin Bredan for excellent editorial assistance. And we would also like to thank Ms. Ans De Beuckelaer for her help with spleen and lymph node isolation. Research in the P.V. group is supported by Belgian grants (Interuniversity Attraction Poles, IAP 7/32), Flemish grants (Research Foundation Flanders: FWO G.0875.11, FWO G.0973.11, FWO G.0A45.12N, FWO G.0787.13N, FWO G.0A54.13N, FWO G.0607.13N, and FWO G0E04.16N), a Methusalem grant (BOF09/01M00709 and BOF16/MET_V/007), Ghent University grants (MRP, GROUP-ID consortium), a grant from the Foundation against Cancer (F2012-188), and grants from VIB. D.V.K. was supported by a FWO postdoctoral grant and is now paid by the Methusalem grant. M.J.M.B. had a tenure track position within the Multidisciplinary Research Program of Ghent University (GROUP-ID) and is now Associate Professor at Ghent University. S.D. and A.D.G. are supported by FWO postdoctoral grants. T.L.A. holds and A.K. held a PhD fellowship from FWO (Research Foundation Flanders).

Received: October 23, 2015
Revised: January 19, 2016
Accepted: March 10, 2016
Published: March 31, 2016

REFERENCES

Apetoh, L., Ghiringhelli, F., Tesniere, A., Obeid, M., Ortiz, C., Criollo, A., Mignot, G., Maiuri, M.C., Ullrich, E., Saulnier, P., et al. (2007). Toll-like receptor 4-dependent contribution of the immune system to anticancer chemotherapy and radiotherapy. Nat. Med. *13*, 1050–1059.

Casares, N., Pequignot, M.O., Tesniere, A., Ghiringhelli, F., Roux, S., Chaput, N., Schmitt, E., Hamai, A., Hervas-Stubbs, S., Obeid, M., et al. (2005). Caspase-dependent immunogenicity of doxorubicin-induced tumor cell death. J. Exp. Med. *202*, 1691–1701.

Cho, Y.S., Challa, S., Moquin, D., Genga, R., Ray, T.D., Guildford, M., and Chan, F.K. (2009). Phosphorylation-driven assembly of the RIP1-RIP3 complex regulates programmed necrosis and virus-induced inflammation. Cell *137*, 1112–1123.

Degterev, A., Huang, Z., Boyce, M., Li, Y., Jagtap, P., Mizushima, N., Cuny, G.D., Mitchison, T.J., Moskowitz, M.A., and Yuan, J. (2005). Chemical inhibitor of nonapoptotic cell death with therapeutic potential for ischemic brain injury. Nat. Chem. Biol. *1*, 112–119.

Denecker, G., Vercammen, D., Steemans, M., Vanden Berghe, T., Brouckaert, G., Van Loo, G., Zhivotovsky, B., Fiers, W., Grooten, J., Declercq, W., and Vandenabeele, P. (2001). Death receptor-induced apoptotic and necrotic cell death: differential role of caspases and mitochondria. Cell Death Differ. *8*, 829–840.

Dondelinger, Y., Aguileta, M.A., Goossens, V., Dubuisson, C., Grootjans, S., Dejardin, E., Vandenabeele, P., and Bertrand, M.J. (2013). RIPK3 contributes to TNFR1-mediated RIPK1 kinase-dependent apoptosis in conditions of cIAP1/2 depletion or TAK1 kinase inhibition. Cell Death Differ. *20*, 1381–1392.

Dynek, J.N., Goncharov, T., Dueber, E.C., Fedorova, A.V., Izrael-Tomasevic, A., Phu, L., Helgason, E., Fairbrother, W.J., Deshayes, K., Kirkpatrick, D.S., and Vucic, D. (2010). c-IAP1 and UbcH5 promote K11-linked polyubiquitination of RIP1 in TNF signalling. EMBO J. *29*, 4198–4209.

Fulda, S. (2014). Therapeutic exploitation of necroptosis for cancer therapy. Semin. Cell Dev. Biol. *35*, 51–56.

Garg, A.D., Krysko, D.V., Vandenabeele, P., and Agostinis, P. (2012a). Hypericin-based photodynamic therapy induces surface exposure of damage-associated molecular patterns like HSP70 and calreticulin. Cancer Immunol. Immunother. *61*, 215–221.

Garg, A.D., Krysko, D.V., Verfaillie, T., Kaczmarek, A., Ferreira, G.B., Marysael, T., Rubio, N., Firczuk, M., Mathieu, C., Roebroek, A.J., et al. (2012b). A novel pathway combining calreticulin exposure and ATP secretion in immunogenic cancer cell death. EMBO J. *31*, 1062–1079.

Ghiringhelli, F., Apetoh, L., Tesniere, A., Aymeric, L., Ma, Y., Ortiz, C., Vermaelen, K., Panaretakis, T., Mignot, G., Ullrich, E., et al. (2009). Activation of the NLRP3 inflammasome in dendritic cells induces IL-1beta-dependent adaptive immunity against tumors. Nat. Med. *15*, 1170–1178.

Hanahan, D., and Weinberg, R.A. (2011). Hallmarks of cancer: the next generation. Cell *144*, 646–674.

He, S., Wang, L., Miao, L., Wang, T., Du, F., Zhao, L., and Wang, X. (2009). Receptor interacting protein kinase-3 determines cellular necrotic response to TNF-alpha. Cell *137*, 1100–1111.

He, L., Peng, K., Liu, Y., Xiong, J., and Zhu, F.F. (2013). Low expression of mixed lineage kinase domain-like protein is associated with poor prognosis in ovarian cancer patients. Onco Targets Ther. *6*, 1539–1543.

Holler, N., Zaru, R., Micheau, O., Thome, M., Attinger, A., Valitutti, S., Bodmer, J.L., Schneider, P., Seed, B., and Tschopp, J. (2000). Fas triggers an alternative, caspase-8-independent cell death pathway using the kinase RIP as effector molecule. Nat. Immunol. *1*, 489–495.

Huang, A.Y.C., Gulden, P.H., Woods, A.S., Thomas, M.C., Tong, C.D., Wang, W., Engelhard, V.H., Pasternack, G., Cotter, R., Hunt, D., et al. (1996). The immunodominant major histocompatibility complex class I-restricted antigen of a murine colon tumor derives from an endogenous retroviral gene product. Proc. Natl. Acad. Sci. USA *93*, 9730–9735.

Jinushi, M., Hodi, F.S., and Dranoff, G. (2008). Enhancing the clinical activity of granulocyte-macrophage colony-stimulating factor-secreting tumor cell vaccines. Immunol. Rev. *222*, 287–298.

Kaczmarek, A., Vandenabeele, P., and Krysko, D.V. (2013). Necroptosis: the release of damage-associated molecular patterns and its physiological relevance. Immunity *38*, 209–223.

Kang, T.B., Yang, S.H., Toth, B., Kovalenko, A., and Wallach, D. (2013). Caspase-8 blocks kinase RIPK3-mediated activation of the NLRP3 inflammasome. Immunity *38*, 27–40.

Kepp, O., Senovilla, L., Vitale, I., Vacchelli, E., Adjemian, S., Agostinis, P., Apetoh, L., Aranda, F., Barnaba, V., Bloy, N., et al. (2014). Consensus guidelines for the detection of immunogenic cell death. OncoImmunology *3*, e955691.

Koo, G.B., Morgan, M.J., Lee, D.G., Kim, W.J., Yoon, J.H., Koo, J.S., Kim, S.I., Kim, S.J., Son, M.K., Hong, S.S., et al. (2015). Methylation-dependent loss of RIP3 expression in cancer represses programmed necrosis in response to chemotherapeutics. Cell Res. *25*, 707–725.

Krysko, D.V., Denecker, G., Festjens, N., Gabriels, S., Parthoens, E., D'Herde, K., and Vandenabeele, P. (2006). Macrophages use different internalization mechanisms to clear apoptotic and necrotic cells. Cell Death Differ. *13*, 2011–2022.

Krysko, D.V., Garg, A.D., Kaczmarek, A., Krysko, O., Agostinis, P., and Vandenabeele, P. (2012). Immunogenic cell death and DAMPs in cancer therapy. Nat. Rev. Cancer *12*, 860–875.

Li, J., McQuade, T., Siemer, A.B., Napetschnig, J., Moriwaki, K., Hsiao, Y.S., Damko, E., Moquin, D., Walz, T., McDermott, A., et al. (2012). The RIP1/RIP3 necrosome forms a functional amyloid signaling complex required for programmed necrosis. Cell *150*, 339–350.

Lohmann, C., Muschaweckh, A., Kirschnek, S., Jennen, L., Wagner, H., and Häcker, G. (2009). Induction of tumor cell apoptosis or necrosis by conditional expression of cell death proteins: analysis of cell death pathways and in vitro immune stimulatory potential. J. Immunol. *182*, 4538–4546.

Ma, Y., Adjemian, S., Mattarollo, S.R., Yamazaki, T., Aymeric, L., Yang, H., Portela Catani, J.P., Hannani, D., Duret, H., Steegh, K., et al. (2013). Anticancer chemotherapy-induced intratumoral recruitment and differentiation of antigen-presenting cells. Immunity *38*, 729–741.

Majno, G., and Joris, I. (1995). Apoptosis, oncosis, and necrosis. An overview of cell death. Am. J. Pathol. *146*, 3–15.

Michaud, M., Martins, I., Sukkurwala, A.Q., Adjemian, S., Ma, Y., Pellegatti, P., Shen, S., Kepp, O., Scoazec, M., Mignot, G., et al. (2011). Autophagy-dependent anticancer immune responses induced by chemotherapeutic agents in mice. Science *334*, 1573–1577.

Murphy, J.M., Czabotar, P.E., Hildebrand, J.M., Lucet, I.S., Zhang, J.G., Alvarez-Diaz, S., Lewis, R., Lalaoui, N., Metcalf, D., Webb, A.I., et al. (2013). The pseudokinase MLKL mediates necroptosis via a molecular switch mechanism. Immunity *39*, 443–453.

Nugues, A.L., El Bouazzati, H., Hétuin, D., Berthon, C., Loyens, A., Bertrand, E., Jouy, N., Idziorek, T., and Quesnel, B. (2014). RIP3 is downregulated in human myeloid leukemia cells and modulates apoptosis and caspase-mediated p65/RelA cleavage. Cell Death Dis. *5*, e1384.

Obeid, M., Panaretakis, T., Joza, N., Tufi, R., Tesniere, A., van Endert, P., Zitvogel, L., and Kroemer, G. (2007a). Calreticulin exposure is required for the immunogenicity of gamma-irradiation and UVC light-induced apoptosis. Cell Death Differ. *14*, 1848–1850.

Obeid, M., Tesniere, A., Ghiringhelli, F., Fimia, G.M., Apetoh, L., Perfettini, J.L., Castedo, M., Mignot, G., Panaretakis, T., Casares, N., et al. (2007b). Calreticulin exposure dictates the immunogenicity of cancer cell death. Nat. Med. *13*, 54–61.

Panaretakis, T., Kepp, O., Brockmeier, U., Tesniere, A., Bjorklund, A.C., Chapman, D.C., Durchschlag, M., Joza, N., Pierron, G., van Endert, P., et al. (2009). Mechanisms of pre-apoptotic calreticulin exposure in immunogenic cell death. EMBO J. *28*, 578–590.

Pasparakis, M., and Vandenabeele, P. (2015). Necroptosis and its role in inflammation. Nature *517*, 311–320.

Pierdomenico, M., Negroni, A., Stronati, L., Vitali, R., Prete, E., Bertin, J., Gough, P.J., Aloi, M., and Cucchiara, S. (2014). Necroptosis is active in children with inflammatory bowel disease and contributes to heighten intestinal inflammation. Am. J. Gastroenterol. *109*, 279–287.

Remijsen, Q., Goossens, V., Grootjans, S., Van den Haute, C., Vanlangenakker, N., Dondelinger, Y., Roelandt, R., Bruggeman, I., Goncalves, A., Bertrand, M.J., et al. (2014). Depletion of RIPK3 or MLKL blocks TNF-driven necroptosis and switches towards a delayed RIPK1 kinase-dependent apoptosis. Cell Death Dis. *5*, e1004.

Sun, L., Wang, H., Wang, Z., He, S., Chen, S., Liao, D., Wang, L., Yan, J., Liu, W., Lei, X., and Wang, X. (2012). Mixed lineage kinase domain-like protein mediates necrosis signaling downstream of RIP3 kinase. Cell *148*, 213–227.

Takemura, R., Takaki, H., Okada, S., Shime, H., Akazawa, T., Oshiumi, H., Matsumoto, M., Teshima, T., and Seya, T. (2015). PolyI:C-induced, TLR3/RIP3-dependent necroptosis backs up immune effector-mediated tumor elimination in vivo. Cancer Immunol. Res. *3*, 902–914.

Vanden Berghe, T., van Loo, G., Saelens, X., Van Gurp, M., Brouckaert, G., Kalai, M., Declercq, W., and Vandenabeele, P. (2004). Differential signaling to apoptotic and necrotic cell death by Fas-associated death domain protein FADD. J. Biol. Chem. *279*, 7925–7933.

Vanlangenakker, N., Vanden Berghe, T., Bogaert, P., Laukens, B., Zobel, K., Deshayes, K., Vucic, D., Fulda, S., Vandenabeele, P., and Bertrand, M.J. (2011). cIAP1 and TAK1 protect cells from TNF-induced necrosis by preventing RIP1/RIP3-dependent reactive oxygen species production. Cell Death Differ. *18*, 656–665.

Vince, J.E., Wong, W.W., Gentle, I., Lawlor, K.E., Allam, R., O'Reilly, L., Mason, K., Gross, O., Ma, S., Guarda, G., et al. (2012). Inhibitor of apoptosis proteins limit RIP3 kinase-dependent interleukin-1 activation. Immunity *36*, 215–227.

Please cite this article in press as: Aaes et al., Vaccination with Necroptotic Cancer Cells Induces Efficient Anti-tumor Immunity, Cell Reports (2016), http://dx.doi.org/10.1016/j.celrep.2016.03.037

Wang, H., Sun, L., Su, L., Rizo, J., Liu, L., Wang, L.F., Wang, F.S., and Wang, X. (2014). Mixed lineage kinase domain-like protein MLKL causes necrotic membrane disruption upon phosphorylation by RIP3. Mol. Cell *54*, 133–146.

Yamazaki, T., Hannani, D., Poirier-Colame, V., Ladoire, S., Locher, C., Sistigu, A., Prada, N., Adjemian, S., Catani, J.P., Freudenberg, M., et al. (2014). Defective immunogenic cell death of HMGB1-deficient tumors: compensatory therapy with TLR4 agonists. Cell Death Differ. *21*, 69–78.

Yatim, N., Jusforgues-Saklani, H., Orozco, S., Schulz, O., Barreira da Silva, R., Reis e Sousa, C., Green, D.R., Oberst, A., and Albert, M.L. (2015). RIPK1 and NF-κB signaling in dying cells determines cross-priming of $CD8^+$ T cells. Science *350*, 328–334.

Zhang, D.W., Shao, J., Lin, J., Zhang, N., Lu, B.J., Lin, S.C., Dong, M.Q., and Han, J. (2009). RIP3, an energy metabolism regulator that switches TNF-induced cell death from apoptosis to necrosis. Science *325*, 332–336.